Characterization of the complex formed by β-glucocerebrosidase and the lysosomal integral membrane protein type-2

Friederike Zunke[a,1], Lisa Andresen[a], Sophia Wesseler[a], Johann Groth[a], Philipp Arnold[b], Michelle Rothaug[a], Joseph R. Mazzulli[c], Dimitri Krainc[c], Judith Blanz[a], Paul Saftig[a], and Michael Schwake[d,1,2]

[a]Institute of Biochemistry, Christian-Albrechts-University of Kiel, 24098 Kiel, Germany; [b]Anatomical Institute, Christian-Albrechts-University of Kiel, 24098 Kiel, Germany; [c]Department of Neurology, Northwestern University Feinberg School of Medicine, Chicago, IL 60611; and [d]Faculty of Chemistry/Biochemistry III, University Bielefeld, 33615 Bielefeld, Germany

Edited by Ellen Sidransky, Medical Genetics Branch, National Human Genome Research Institute, National Institutes of Health, Bethesda, MD, and accepted by the Editorial Board February 24, 2016 (received for review July 21, 2015)

The lysosomal integral membrane protein type-2 (LIMP-2) plays a pivotal role in the delivery of β-glucocerebrosidase (GC) to lysosomes. Mutations in GC result in Gaucher's disease (GD) and are the major genetic risk factor for the development of Parkinson's disease (PD). Variants in the LIMP-2 gene cause action myoclonus-renal failure syndrome and also have been linked to PD. Given the importance of GC and LIMP-2 in disease pathogenesis, we studied their interaction sites in more detail. Our previous data demonstrated that the crystal structure of LIMP-2 displays a hydrophobic three-helix bundle composed of helices 4, 5, and 7, of which helix 5 and 7 are important for ligand binding. Here, we identified a similar helical motif in GC through surface potential analysis. Coimmunoprecipitation and immunofluorescence studies revealed a triple-helical interface region within GC as critical for LIMP-2 binding and lysosomal transport. Based on these findings, we generated a LIMP-2 helix 5-derived peptide that precipitated and activated recombinant wild-type and GD-associated N370S mutant GC in vitro. The helix 5 peptide fused to a cell-penetrating peptide also activated endogenous lysosomal GC and reduced α-synuclein levels, suggesting that LIMP-2–derived peptides can be used to activate endogenous as well as recombinant wild-type or mutant GC efficiently. Our data also provide a structural model of the LIMP-2/GC complex that will facilitate the development of GC chaperones and activators as potential therapeutics for GD, PD, and related synucleinopathies.

LIMP-2 | Gaucher's disease | β-glucocerebrosidase | GC activators | Parkinson's disease

The lysosomal glucosidase β-glucocerebrosidase (GC) is required for hydrolysis of glucosylceramide and is targeted to lysosomes in a mannose-6 phosphate–independent manner by the lysosomal integral membrane protein type-2 (LIMP-2) (1, 2). Interaction of the two proteins occurs in the endoplasmic reticulum (ER) (1, 3), followed by trafficking of the LIMP-2/GC complex to lysosomes. Mutations in LIMP-2 cause action myoclonus-renal failure (AMRF) (4). LIMP-2 mutants linked to AMRF localize to the ER (3), causing missorting and lysosomal depletion of GC, highlighting the importance of functional LIMP-2 for correct targeting of GC. Reduced lysosomal activity of GC also is a hallmark of Gaucher`s disease (GD), which is caused by mutations in GC. Although only a few AMRF-causing mutations are known for LIMP-2, more than 300 mutations within GC, affecting the activity, stability, and/or the intracellular distribution of the enzyme, have been described (5). Patients carrying mutations in GC have an increased risk of developing synucleinopathies including Parkinson`s disease (PD) and dementia with Lewy bodies (6, 7). Importantly, a reduction in GC activity also is found in patients with sporadic PD (8). We recently showed reduced neuronal GC activity and increased α-synuclein in LIMP-2–deficient mice that also exhibited severe neurological deficits (9). These findings are supported by a significant association of genetic variations in the LIMP-2 locus with dementia with Lewy bodies (10) and emphasize the involvement of the LIMP-2–mediated lysosomal transport of GC in the pathogenesis of synucleinopathies. Augmentation of GC activity in murine brain of GD and PD mouse models led to a reduction of α-synuclein accumulation and amelioration of neuronal pathology (11, 12). Several hypotheses suggest a link between mutated GC and dysregulated α-synuclein homeostasis (13). For example, the GC substrate glucosylceramide has been proposed to promote α-synuclein accumulation by exerting a stabilizing effect on toxic oligomeric forms of α-synuclein (14). A feedback loop in which accumulated α-synuclein partially blocks the ER-to-Golgi transport of GC was suggested to increase this pathological cascade further (14).

The recently solved crystal structure of the LIMP-2 ectodomain revealed an exposed three-helix bundle, which is formed by helices 4, 5, and 7; helices 5 and 7 likely serve as a GC-binding domain (15). Because the secondary structure and hydrophobicity of this region are important for binding and intracellular transport of GC (1), we hypothesized that GC might harbor a similar motif necessary for LIMP-2 binding. Here, we describe the identification and characterization of a hydrophobic helical interface within GC, mediating binding to LIMP-2. We therefore suggest a model of LIMP-2/GC interaction that may be important for the design of small-molecule GC activators. Furthermore, we generated a LIMP-2–derived helical peptide that can be used to purify, activate, and stabilize GC in vitro as well as in cell-based assays. Our data also

Significance

Apart from the lysosomal integral membrane protein type-2 (LIMP-2)–dependent trafficking of β-glucocerebrosidase (GC) to lysosomes, little is known about the interaction of LIMP-2 and GC on the molecular level. The structural and biochemical characterization of LIMP-2/GC interaction sites has potential importance for the design of GC-activating compounds. We show that a LIMP-2–derived helical peptide can be used for efficient purification and activation of recombinant and endogenous GC. These results provide a molecular framework for the design of GC activators as potential treatments in Parkinson's disease and related synucleinopathies.

Author contributions: F.Z. and M.S. designed research; F.Z., L.A., S.W., J.G., P.A., M.R., and J.B. performed research; J.R.M. contributed new reagents/analytic tools; F.Z. and M.S. analyzed data; and F.Z., D.K., J.B., P.S., and M.S. wrote the paper.

The authors declare no conflict of interest.

This article is a PNAS Direct Submission. E.S. is a guest editor invited by the Editorial Board.

[1]Present address: Department of Neurology, Northwestern University Feinberg School of Medicine, Chicago, IL 60611.

[2]To whom correspondence should be addressed. Email: michael.schwake@uni-bielefeld.de.

This article contains supporting information online at www.pnas.org/lookup/suppl/doi:10.1073/pnas.1514005113/-/DCSupplemental.

suggest that this chaperone-like activity of LIMP-2 could increase lysosomal targeting of wild-type or mutant forms of GC, thereby decreasing intralysosomal accumulation of glucosylceramide in synucleinopathies.

Results

LIMP-2 and GC Interaction Is Mediated by Hydrophobic Helical Interfaces on both Proteins. Previous mutagenesis studies, guided by the crystal structure of the LIMP-2 ectodomain, indicated that the hydrophobic helices 5 and 7 are critical for an interaction with GC (15). Consistent with these findings, we show here that mutations within helix 5 and 7 of LIMP-2 that reduced the hydrophobicity of this region (Fig. S1 *A* and *B*) impaired the ability to rescue reduced GC activity in a LIMP-2–deficient cell system (Fig. S1*C*). Thus we confirm in a cellular model that the hydrophobicity of the helical bundle in LIMP-2 is critical for binding and intracellular transport of GC. Because the interaction domain within the GC protein is unknown, we used the available crystal structure of GC (16, 17) and surface potential analysis to identify potential GC/LIMP-2 interaction sites in silico (Fig. 1*A*). A potential interaction region in GC, which consisted of a hydrophobic helical interface (white area in Fig. 1*A*) and is composed of three helices, 1a, 1b, and 2 (Fig. 1*B*), was identified by its similarity to helices 5 and 7 of LIMP-2.

To determine if these helices are important for binding to LIMP-2, we substituted single amino acids within this helical motif by replacing conserved hydrophobic leucines with negatively charged glutamic acids (Fig. 1 *B* and *C*). This substitution resulted in the three GC mutants L91E (helix 1a), L94E (helix 1a), and L156E (helix 2). A R211E GC mutant served as a control because this mutation is located outside the identified hydrophobic helical motif (Fig. 1*B*). The GC mutants were expressed in cells and assayed for their ability to bind LIMP-2 by coimmunoprecipitation (co-IP). In contrast to wild-type GC and the control mutant R211E, the three point mutations within the helical motif of GC impaired co-IP with LIMP-2 (Fig. 1 *D* and *E*). Immunofluorescence (IF) studies demonstrated the colocalization of wild-type

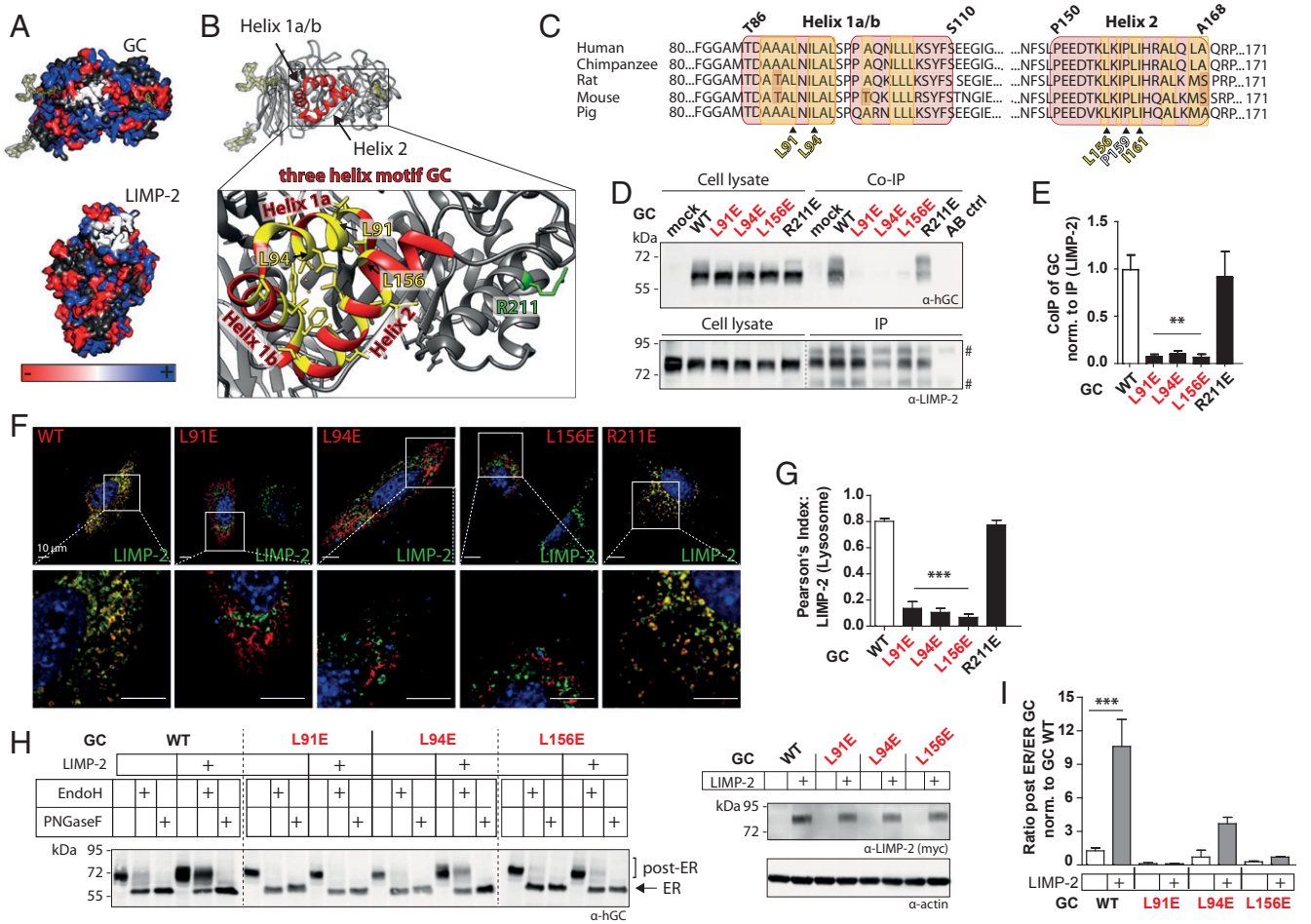

Fig. 1. Identification of the LIMP-2 interaction site in GC by structural and molecular analyses. (*A*) Illustration of surface charges in LIMP-2 [Protein Data Bank (PDB) ID code 4F7B] and GC (PDB ID code 2J25). Hydrophobic areas are shown in white. (*B*, *Upper*) Protein structure of GC (PDB ID code 2J25) with a hydrophobic patch (shown in red) revealing three helices: helix 1a, helix 1b, and helix 2. (*Lower*) Magnification of the helical region. Hydrophobic amino acids are indicated in yellow. (*C*) Sequence alignment of multiple GC species (red boxes: helix1a/b and 2; yellow: hydrophobic residues). (*D*) Co-IP of overexpressed GC helix mutants L91E, L94E, and L156E and wild-type and control R211E mutant in N2a cells using a LIMP-2– (immunoprecipitated) and a human GC-specific antibody (α-hGC). #, bands from denatured antibody used for IP; AB ctrl, antibody control. The dotted line indicates different exposure times of the same immunoblot. (*E*) Densitometric quantification of bound GC protein normalized to precipitated LIMP-2 ($n = 4$–12). (*F*) IF of GC-deficient cells transfected with the GC helical motif mutants (L91E, L94E, and L156E) and control R211E mutant (α-hGC; red), costained for endogenous LIMP-2 (green). The areas of magnification in the lower row are outlined by white boxes in the upper row. (*G*) Colocalization of GC and LIMP-2 was determined using the Pearson's index ($n = 4$–10). (*H* and *I*) Immunoblot (*H*) and densitometric quantification (*I*) (post-ER/ER ratio normalized to wild-type GC; $n = 2$ or 3) of EndoH- or PNGaseF-treated cell extracts of GC-deficient cells expressing GC mutants L91E, L94E, and L156E and wild-type GC (α-hGC) with or without myc-tagged LIMP-2 (α-myc). Actin was used as loading control. EndoH resistance of proteins indicates their post-ER localization. Dotted lines in *H* separate individual blots. $^{**}P < 0.01$; $^{***}P < 0.001$. See also Fig. S1.

GC and the R211E mutant with endogenous LIMP-2 (Fig. 1 *F* and *G*) and lysosome-associated membrane glycoprotein 2 (LAMP-2) (Fig. S1 *D* and *E*) in lysosomes, whereas the GC helical motif mutants L91E, L94E, and L156E remained in the ER (Fig. S1 *F* and *G*). Furthermore a colocalization of wild-type GC with overexpressed LIMP-2 also was found in lysosomes but was reduced significantly upon expression of the GC mutants L91E and L156E (Fig. S1 *H* and *I*). To evaluate the cellular fate of the GC helical motif mutants further, we used GC-deficient mouse embryonic fibroblasts (MEFs) (Fig. 1 *H* and *I*) and murine neuroblastoma (N2a) cells (Fig. S1 *J* and *K*) for endoglycosidase H (EndoH) and peptide-*N*-glycosidase F (PNGaseF) treatment of cellular extracts. Although PNGaseF removes all N-linked glycans from GC and served as a control to detect unglycosylated GC, EndoH discriminates between mature (EndoH-insensitive) and immature (EndoH-sensitive) N-linked glycans. Thus, complete EndoH-sensitive bands indicate the ER localization of GC. Overexpression of wild-type GC in GC-deficient MEFs and N2a cells resulted in a small fraction of post-ER forms of GC (Fig. 1*H* and Fig. S1*J*; see the EndoH-treated sample in the second lane). Coexpression of LIMP-2 caused a 10-fold increase in the post-ER form of wild-type GC (Fig. 1 *H*, lane 5, and *I*, and Fig. S1 *J*, lane 5, and *K*). In contrast, LIMP-2 overexpression did not alter the post-ER levels of the GC helical motif mutants L91E and L156E and altered the post-ER levels of the L94E GC mutant only to a minor degree (Fig. 1 *H* and *I* and Fig. S1 *J* and *K*). This result indicates some residual interaction of LIMP-2 with the L94E mutant under more native cellular conditions. The residual interaction found here was not detected by the previous co-IP experiments (Fig. 1 *D* and *E*), possibly because of the stringency of the applied co-IP buffer. We then evaluated whether the observed increase in GC maturation also leads to changes in its enzymatic activity. Upon coexpression of wild-type GC and LIMP-2, we observed a significant increase in GC activity, which was not evident for the three GC helical motif mutants L91E, L94E, and L156E (Fig. S1*L*). Overall our data suggest that the hydrophobicity of a three-helix motif within GC is critical for proper LIMP-2 binding. Furthermore, LIMP-2 expression appears to be a limiting factor for ER exit and post-ER trafficking of GC.

Identification of GD-Causing Mutations Within the Three-Helix Motif of GC and Their Interference with LIMP-2 Binding. To evaluate if GD-associated mutations within the potential binding motif of GC might interfere with LIMP-2 interactions, we analyzed two GD mutants, P159L and I161S. Both mutations are located within helix 2 of the hydrophobic helical interface (Figs. 1*C* and 2*A*) (5, 18). As a control, we used two additional mutants, obtained from GD patients, F213I and N188S (5, 19), which reside outside the hydrophobic helical motif of GC and thus should not interfere with LIMP-2 interactions (Fig. 2*A*). We first analyzed LIMP-2 binding

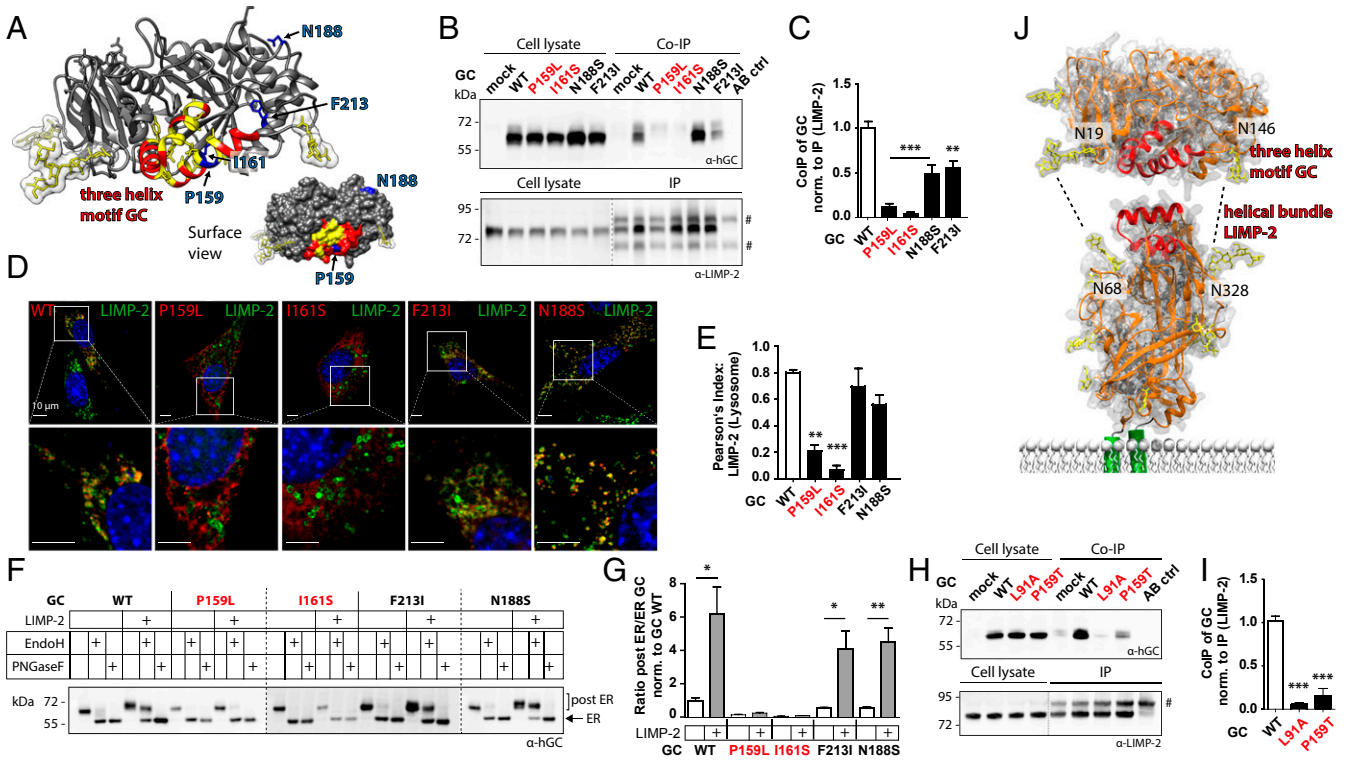

Fig. 2. Analysis of the LIMP-2 interaction site in GC mutants obtained from GD patients. (*A*) Structure of GC (PDB ID code 2J25); helical motif and hydrophobic amino acids are highlighted in red and yellow, respectively. The clinically relevant GC mutants obtained from GD patients, P159L and I161S (located in helix 2) and F213I and N188S (outside the helical motif), are depicted in blue. A surface view shows surface exposure of indicated amino acids. (*B*) Co-IP of the GC mutants found in GD patients, P159L, I161S, F213I, and N188S (α-hGC), expressed in N2a cells. A LIMP-2 antibody was used for IP. #, bands from denatured antibody used for IP; AB ctrl, antibody control. The dotted line indicates different exposure times of the same immunoblot. (*C*) Densitometry of co-IP studies (normalized to LIMP-2) ($n = 4$–11). (*D*) IF costaining of GC mutants (α-hGC; red) expressed in GC-deficient cells with endogenous LIMP-2 (green). The areas of magnification in the lower row are indicated by white boxes in the upper row. (*E*) Pearson's index give the degree of GC–LIMP-2 colocalization ($n = 3$–10). (*F* and *G*) Immunoblot (*F*) and densitometric quantification (*G*) of GC mutants found in GD patients (α-hGC) with and without coexpression of LIMP-2 in GC-deficient cells treated with EndoH or PNGaseF. The post-ER/ER ratio is normalized to wild-type GC ($n = 3$). In *F*, the upper EndoH-resistant band of GC indicates the post-ER location of the protein; the lower band corresponds to ER residence. (*H*) Co-IP of L91A and GC mutant P159T (found in a GD patient) overexpressed in N2a cells (α-hGC). The dotted line indicates different exposure time of same immunoblot. (*I*) Quantification of bound GC protein normalized to precipitated LIMP-2 ($n = 4$–5). (*J*) Binding model of LIMP-2 and GC with potential stabilizing interaction of carbohydrate chains of both proteins (dotted lines). $^*P < 0.05$; $^{**}P < 0.01$; $^{***}P < 0.001$. See also Fig. S2.

of these mutants and then the LIMP-2–dependent intracellular transport of GC. Co-IP experiments revealed impaired binding of the GC mutants P159L and I161S to LIMP-2 as compared with wild-type GC (Fig. 2 *B* and *C*). The two control mutants F213I and N188S still bound to LIMP-2, albeit to a reduced extent compared with wild-type GC (Fig. 2 *B* and *C*). IF microscopy in GC-deficient cells demonstrated decreased lysosomal transport of the hydrophobic helix mutants P159L and I161S (Fig. 2 *D* and *E* and Fig. S2 *A* and *B*). In contrast the two control mutants F213I and N188S still colocalized with LIMP-2 (Fig. 2 *D* and *E*) and LAMP-2 (Fig. S2 *A* and *B*), indicating their lysosomal localization. Furthermore, colocalization with protein disulfide-isomerase (PDI) revealed increased ER localization of the two GD mutants P159L and I161S compared with wild-type GC or the control mutant N188S (Fig. S2 *C* and *D*). In addition the two GD-associated helix mutants P159L and I161S showed significantly reduced colocalization with overexpressed LIMP-2, but the control mutants F213I and N188S did not (Fig. S2 *E* and *F*). An EndoH digest confirmed the retention of the clinical mutants P159L and I161S within the ER, whereas the GC mutants F213I and N188S were found in post-ER fractions (Fig. 2 *F* and *G*). In addition, overexpression of LIMP-2 did not increase the post-ER transport of the P159L and I161S, mutants as observed for the F123 and N188S mutants (Fig. 2 *F* and *G*), strengthening our hypothesis that the P159L and I161S mutants are incapable of binding to LIMP-2 via their hydrophobic helical motif, thus resulting in decreased ER exit and lysosomal transport.

To characterize the LIMP-2–binding domain further, we analyzed two additional GC mutants, the GD-associated point mutation P159T, which carries a polar threonine at position 159, and the L91A mutant carrying an alanine at position 91, which represents a hydrophobic amino acid but has a less bulky side chain than the original leucine. Both mutations resulted in impaired binding of mutated GC to LIMP-2 as revealed by co-IP studies (Fig. 2 *H* and *I*), further indicating the importance of single amino acids for LIMP-2 binding in this highly conserved region. Importantly, all GC mutants analyzed so far in this study exhibited expression levels comparable with that of the wild-type enzyme (Figs. 1*D* and 2*B*, Upper, and Fig. S2*G*).

In summary, our findings suggest that the LIMP-2–binding region in GC is located in a helical interface formed by helix 1a (residues T86–L96), helix 1b (residues P99–S110), and helix 2 (P150–A168), displaying a hydrophobic patch similar to that found in LIMP-2. Therefore, we propose a model in which GC and LIMP-2 interact via two hydrophobic helical interfaces (Fig. 2*J*, Fig. S2*H*, and Movie S1). Consistent with this model, a crystal structure of LIMP-2 solved at pH 5.5 (20) shows a large conformational change in the identified binding site of helix 5; this change likely is responsible for the dissociation of GC at low lysosomal pH (Fig. S2*H*).

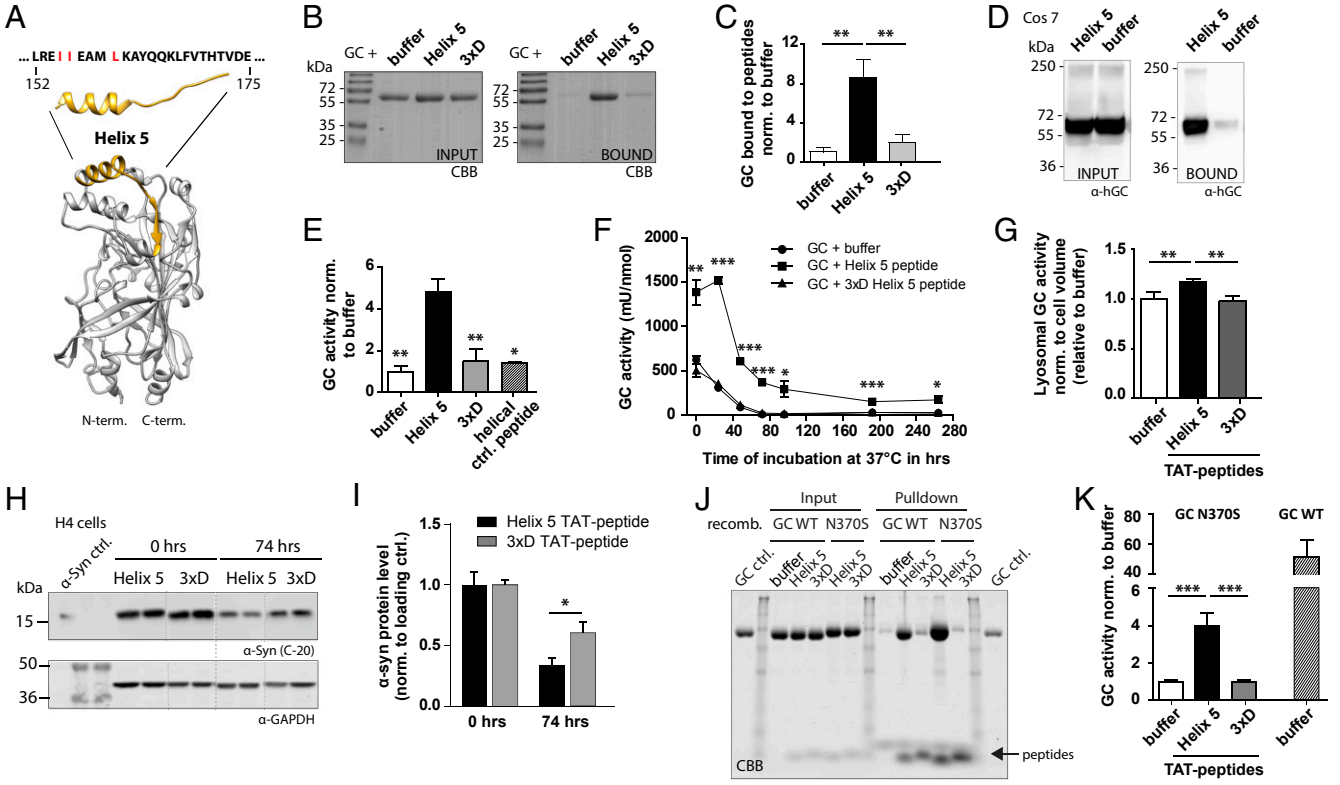

Fig. 3. Structural characteristics of LIMP-2–derived peptide comprised of helix 5 and its effect on GC function. (*A*) Protein structure of LIMP-2 (PDB ID code 4F7B) with the helix 5 peptide sequence (L152–E175) highlighted. Amino acids in red [two isoleucines (I) and one leucine (L)] were replaced by aspartic acid (3×D). (*B* and *C*) Pulldown (*B*) and densitometry (*C*) of recombinant GC bound to peptides (helix 5 or 3×D) relative to the bound protein fraction of buffer control ($n = 4$–5). Proteins were visualized by Coomassie staining (CBB). (*D*) Immunoblot of endogenous GC in Cos 7 cells (α-hGC) after pulldown with the helix 5 peptide. (*E*) Assay of the GC activity of recombinant GC incubated with helix 5 or 3×D peptide ($n = 4$). (*F*) Stabilization assay of GC mixed with buffer, helix 5, or 3×D peptide incubated at 37 °C for 270 h ($n = 3$). (*G*) Lysosomal GC activity of living H4 cells measured in vivo after incubation with uptake-optimized TAT peptides (helix 5 and 3×D). GC activity was normalized to cell volume and is shown relative to buffer control ($n = 4$). (*H* and *I*) TAT peptide uptake (helix 5 and 3×D) in H4 cells, stably overexpressing α-synuclein under a tetracycline-inducible promoter in conjunction with doxycycline to stop de novo synthesis of α-synuclein (α-Syn). Immunoblot (*H*) and densitometry analysis (*I*) of the α-synuclein level (normalized to loading control) after 74 h of incubation with helix 5 TAT peptide. The value at incubation time t_0 was set as 1 ($n = 6$). (*J*) Pulldown of recombinant wild-type GC and the GC N370S mutant with TAT peptides (helix 5 and 3×D). (*K*) Activity assay of recombinant mutant N370S GC after incubation with TAT peptides (helix 5 and 3×D). As a reference value, wild-type GC activity is shown on the right. GC activity was normalized to buffer control ($n = 3$–5). See also Fig. S3.

A Synthetic LIMP-2–Derived Peptide Is Sufficient to Interact with GC and Increases the Enzymatic Activity. We then asked if helix 5, the most apically exposed helix of LIMP-2, is sufficient for binding to GC. To this end, we generated a LIMP-2–derived helix 5 peptide together with a control peptide with two isoleucine and one leucine residues replaced by three aspartates (3×D) (Fig. 3*A*). We have shown previously that a LIMP-2 mutant containing these three aspartates failed to bind GC (3). Circular dichroism spectroscopy confirmed the helical structure of the helix 5 peptide, but the control peptide was nonhelical (Fig. S3*A*). Both peptides were N-terminally tagged with biotin and used for GC pulldown experiments at neutral pH. After the peptides were incubated with either recombinant GC (Fig. 3 *B* and *C*) or cellular lysates (Fig. 3*D*), only the wild-type helix 5 peptide specifically coprecipitated recombinant as well as endogenous GC. In addition, no interaction of the helix 5 peptide with recombinant α-mannosidase (LAMAN), a lysosomal hydrolase, or albumin (BSA) could be detected (Fig. S3 *B* and *C*), demonstrating the specific interaction of this helix 5 peptide with GC.

To address the functional impact of the observed interaction between the helix 5 peptide and recombinant GC, we measured GC activity in the presence of a one- to 10-fold molar excess of the helix 5 peptide (Fig. S3*D*). Enzyme activity was increased five times in the presence of a 10-fold molar excess of the helix 5 peptide, whereas the 3×D control peptide did not increase the GC activity (Fig. 3*E*). A random helical control peptide consisting of 24 amino acids (21) also was unable to increase GC activity, further supporting the specificity of the helix 5 peptide (Fig. 3*E*). The purified luminal domain of LIMP-2 had a similar effect on GC activity (Fig. S3*D*), suggesting that the activating effect of LIMP-2 on GC is mediated mainly by helix 5. No effect on LAMAN enzymatic activity was detected after incubation with the helix 5 peptide or the LIMP-2 ectodomain, further emphasizing the specificity of the helix 5 peptide on GC activity (Fig. S3*E*). The enzymatic activity of endogenous and overexpressed GC in cell lysates also was increased after incubation with the helix 5 peptide (Fig. S3*F*). To analyze if the increase in GC activity is caused by the stabilization of the enzyme, recombinant GC was incubated with the helix 5 and the control peptide at 37 °C, and the activity of GC was measured at regular intervals (Fig. 3*F*). Incubation of GC with buffer alone or the control 3×D peptide led to a complete loss of enzymatic activity within 72 h, whereas GC still displayed significant enzymatic activity in presence of the helix 5 peptide (helix 5: $t_{1/2}$ = 48 h; 3×D: $t_{1/2}$ = 24 h) (Fig. 3*F*).

We also analyzed if the helix 5 peptide-mediated increase in GC activity measured in vitro could be detected in lysosomes of living cells. To facilitate cellular uptake of the peptide, we used a cell-penetrating helix 5 and a control peptide (3×D) that were C-terminally linked with a HIV-derived TAT motif (22). We also added the chaperone-mediated autophagy-targeting motif KFERQ to support lysosomal import of these peptides (23). This effect of helix 5 peptide, as well as the control (3×D) TAT peptide, on recombinant GC activity was comparable to the effect observed for the unmodified peptides (Fig. S3*G*). Using IF, we detected the helix 5 TAT peptide in vesicular structures that partly colocalized with LIMP-2 in H4 human neuroglioma cells, indicating lysosomal localization (Fig. S3*H*). Next, using a compartment-specific activity assay (24), we confirmed that the helix 5 TAT peptide could elevate GC activity directly within lysosomes of living cells by ∼18% (Fig. 3*G* and Fig. S3*I*). Because it has been demonstrated previously that elevated GC activity reduces α-synuclein levels (9, 11, 12), we investigated the effect of the helix 5 TAT peptide on the clearance of α-synuclein in H4 cells stably overexpressing wild-type α-synuclein under a tetracycline-inducible promoter. These cells were incubated with the helix 5 or the control (3×D) TAT peptide and were treated with doxycycline to suppress de novo α-synuclein synthesis. Cells were harvested at 0 and 74 h after doxycycline addition, and the remaining α-synuclein levels were analyzed by Western blot. Enhancement of GC activity persisted for the 74-h time course of the assay with the helix 5 TAT peptide but not with the control 3×D TAT peptide (Fig. S3*J*). A significant reduction in α-synuclein levels was observed 74 h after incubation with the helix 5 TAT peptide, as compared with the 3×D control peptide (Fig. 3 *H* and *I*). To evaluate the therapeutic potential of the LIMP-2–derived helix 5 peptide further, we assessed its effect on the recombinant GC mutant N370S, which represents one of the most prevalent GD-causing mutations with low catalytic activity (25, 26). Using a cell-free system, we found that recombinant N370S mutant GC could be precipitated by the helix 5 TAT peptide as efficiently as recombinant wild-type GC (Fig. 3*J*); this finding is consistent with the localization of the N370S mutation outside the three helical LIMP-2–binding motif (Fig. S3*K*). Furthermore, similar to its effect on wild-type GC (Fig. 3*E*), the helix 5 TAT peptide led to a fourfold increase in the activity of the N370S mutant (Fig. 3*K*).

Our data provide evidence that the interaction site of LIMP-2 and GC consists of two hydrophobic helical interfaces. The integrity of these helical motifs on both proteins is critical for LIMP-2–mediated lysosomal transport of GC. Additionally, a LIMP-2–derived helix 5 peptide is sufficient for binding and activating both wild-type and mutant GC in vitro and in cell-based assays. We propose binding of the LIMP-2–derived helix 5 peptide to the hydrophobic three-helix motif found on GC as described for LIMP-2 (Fig. S3*K* and Movie S1). The characterization of this interaction site on GC might have important implications for the future drug design of GC activators.

Discussion

The determination of the crystal structures of LIMP-2 (15) and GC (16) and their respective binding sites revealed here provides a deeper understanding of how this receptor/ligand protein complex triggers transport of GC to the lysosomal compartment. Our data suggest that LIMP-2 and GC interact via two helical interfaces in a 1:1 stoichiometry, as is consistent with our previous crosslinking experiments (1). The described helical interfaces on LIMP-2 and GC expose mainly hydrophobic side chains, indicating a hydrophobic interaction. This notion is supported by our findings that introduction of negatively charged amino acids in either helical interface impaired LIMP-2 binding to GC. The two clinically relevant GC mutations in helix 2 support this mode of interaction, because the I161S mutation decreases the hydrophobicity and the P159L mutant interferes with the secondary structure of the helical motif of GC or neighboring protein structures. Interestingly, the hydrophobic helical motif is found opposite the catalytic cavity and also opposite the proposed saposin C-binding site (27, 28), suggesting that LIMP-2/GC interaction does not interfere with the binding of saposin C. Furthermore, in agreement with our previous findings of a glycosylation-independent LIMP-2/GC interaction (1, 3), the LIMP-2/GC interaction site does not harbor glycosylation sites. Our data propose a model in which sugar chains of both proteins come in close contact upon complex formation (Fig. 2*J*), potentially exerting a stabilizing effect on the LIMP-2/GC protein complex and thereby assisting in the lysosomal transport of the enzyme. Interestingly, very few GD-causing mutations in GC have been reported within this interface region so far (5). It is possible that such mutations do not affect the catalytic activity of GC but rather diminish its binding to LIMP-2, leading to the secretion and recapture of a still functional enzyme via endocytosis. The amount of GC reaching lysosomes through this indirect pathway could be sufficient for several cell types to degrade sphingolipids (e.g., macrophages), as demonstrated by the successful application of exogenous recombinant GC in enzyme-replacement therapy (29–31).

Recently, Liou et al. (32) proposed that the LIMP-2–binding motif in GC consists of an 11-amino acid stretch that forms a surface-accessible loop in the close vicinity of the helical interface reported here. However, most of the residues within this loop that are mutated in this study point toward the core of GC, suggesting they have a secondary effect on the helical motif rather than affecting binding directly.

We found that a LIMP-2–derived helix 5 peptide sufficiently binds to the helical motif of GC leading to a fivefold increase of recombinant GC activity. The use of this helix 5-derived peptide could offer a previously unidentified strategy to purify GC efficiently from cell-culture medium or cell lysates. Moreover, this helix 5-derived LIMP-2 peptide could be exploited as an activator of wild-type and even mutant GC. The underlying mechanism of the helix 5 peptide-mediated GC activation remains to be established, but our in vitro assays already indicate that the peptide has a stabilizing effect on the enzyme. We propose the helix 5 peptide binds to the same hydrophobic interface of GC as described for LIMP-2 in this study. Most of the recently described chaperones of GC are inhibitors of the enzyme (33, 34). In contrast, we propose here that the binding site of the helix 5 peptide resides outside the catalytic cavity of GC. Thus, we assume that the bound helix 5 peptide has an allosteric, noninhibitory effect on GC activity.

In summary, our study describes a helix motif in GC responsible for the interaction with LIMP-2 and presents a model of the receptor/ligand complex. It also reveals an activating effect of a small LIMP-2–derived peptide on GC. Identification of the peptide binding at this particular region on GC further opens the possibility of designing small molecules to target this domain. Understanding the LIMP-2 interaction site in GC may further elucidate the molecular aspects of GD and AMRF and help optimize therapeutic strategies for patients. Preserving or enhancing LIMP-2/GC interaction will be important in therapeutic efforts geared toward the development of activators and chaperones of LIMP-2 or GC.

Experimental Procedures

Expression plasmids of LIMP-2 and human GC constructs (Table S1) were generated as described previously (1). For the cell lines used, please refer to *SI Experimental Procedures* and Table S2. For Western blotting nitrocellulose or PVDF membranes were used. EndoH/PNGaseF digests were performed according to the manufacturer's instructions (New England Biolabs). For co-IP experiments magnetic agarose G beads (Thermo Fisher Scientific) were used. For more information refer to *SI Experimental Procedures*. IF studies were performed in cells as previously described (1, 3). Cellular colocalization of two proteins was determined by Pearson's index (35) (also see *SI Experimental Procedures*). Enzyme activity assays of cell lysates or recombinant protein were measured at acid pH using absorbent and fluorescent artificial substrates; for further information see *SI Experimental Procedures*. For peptide studies, peptides were N-terminally tagged with biotin. If not stated otherwise, recombinant enzyme was incubated with a 10-fold higher molarity of peptides. Conditions for pulldown experiments were kept at neutral pH. More information can be found in *SI Experimental Procedures*. Protein modeling, molecular analyses, graphics, and animations were performed with the University of California, San Francisco Chimera package (www.cgl.ucsf.edu/chimera) supported by National Institute of General Medical Sciences Grant P41-GM103311.

Primers used for cloning and site-directed mutagenesis are given in Table S3; antibodies used are listed in Table S4; peptide sequences are provided in Table S5; buffers, solutions, and recombinant proteins are described in Table S6; and the settings for CD spectroscopy are detailed in Table S7.

For statistical analyses, all values are expressed as the mean ± SEM and were analyzed via a two-sided, unpaired Student's *t* test or one-way ANOVA followed by a Tukey–Kramer multiple comparison test using GraphPad Instat 3 software when multiple samples were analyzed. In all analyses the null hypothesis was rejected at $P < 0.05$ (*$P < 0.05$, **$P < 0.01$, ***$P < 0.001$). If not indicated otherwise, significant differences in the graphs show GC/LIMP-2 mutants compared with each respective wild-type or buffer/control peptides compared with the helix 5 peptide.

ACKNOWLEDGMENTS. We thank Ellen Sidransky and Pamela McLean for the β-glucocerebrosidase (GC)-deficient mouse embryonic fibroblasts and H4 cells, respectively, and Johannes Aerts (Leiden University) for the GC antibody and for critically reading the manuscript. This work was supported by a Böhringer Ingelheim Fonds Fellowship (to F.Z.), a Deutsche Forschungsgemeinschaft (DFG) Heisenberg fellowship (to M.S.), and DFG Grants GRK1459 (to M.S. and J.B.), R01NS076054 (to D.K.), and R01NS092823 (to J.R.M.).

1. Reczek D, et al. (2007) LIMP-2 is a receptor for lysosomal mannose-6-phosphate-independent targeting of beta-glucocerebrosidase. *Cell* 131(4):770–783.
2. Blanz J, et al. (2015) Mannose 6-phosphate-independent Lysosomal Sorting of LIMP-2. *Traffic* 16(10):1127–1136.
3. Blanz J, et al. (2010) Disease-causing mutations within the lysosomal integral membrane protein type 2 (LIMP-2) reveal the nature of binding to its ligand beta-glucocerebrosidase. *Hum Mol Genet* 19(4):563–572.
4. Berkovic SF, et al. (2008) Array-based gene discovery with three unrelated subjects shows SCARB2/LIMP-2 deficiency causes myoclonus epilepsy and glomerulosclerosis. *Am J Hum Genet* 82(3):673–684.
5. Hruska KS, LaMarca ME, Scott CR, Sidransky E (2008) Gaucher disease: Mutation and polymorphism spectrum in the glucocerebrosidase gene (GBA). *Hum Mutat* 29(5):567–583.
6. Nalls MA, et al. (2013) A multicenter study of glucocerebrosidase mutations in dementia with Lewy bodies. *JAMA Neurol* 70(6):727–735.
7. Westbroek W, Gustafson AM, Sidransky E (2011) Exploring the link between glucocerebrosidase mutations and parkinsonism. *Trends Mol Med* 17(9):485–493.
8. Gegg ME, et al. (2012) Glucocerebrosidase deficiency in substantia nigra of parkinson disease brains. *Ann Neurol* 72(3):455–463.
9. Rothaug M, et al. (2014) LIMP-2 expression is critical for β-glucocerebrosidase activity and α-synuclein clearance. *Proc Natl Acad Sci USA* 111(43):15573–15578.
10. Bras J, et al. (2014) Genetic analysis implicates APOE, SNCA and suggests lysosomal dysfunction in the etiology of dementia with Lewy bodies. *Hum Mol Genet* 23(23):6139–6146.
11. Sardi SP, et al. (2011) CNS expression of glucocerebrosidase corrects alpha-synuclein pathology and memory in a mouse model of Gaucher-related synucleinopathy. *Proc Natl Acad Sci USA* 108(29):12101–12106.
12. Sardi SP, et al. (2013) Augmenting CNS glucocerebrosidase activity as a therapeutic strategy for parkinsonism and other Gaucher-related synucleinopathies. *Proc Natl Acad Sci USA* 110(9):3537–3542.
13. Siebert M, Sidransky E, Westbroek W (2014) Glucocerebrosidase is shaking up the synucleinopathies. *Brain* 137(Pt 5):1304–1322.
14. Mazzulli JR, et al. (2011) Gaucher disease glucocerebrosidase and α-synuclein form a bidirectional pathogenic loop in synucleinopathies. *Cell* 146(1):37–52.
15. Neculai D, et al. (2013) Structure of LIMP-2 provides functional insights with implications for SR-BI and CD36. *Nature* 504(7478):172–176.
16. Brumshtein B, Wormald MR, Silman I, Futerman AH, Sussman JL (2006) Structural comparison of differently glycosylated forms of acid-beta-glucosidase, the defective enzyme in Gaucher disease. *Acta Crystallogr D Biol Crystallogr* 62(Pt 12):1458–1465.
17. Dvir H, et al. (2003) X-ray structure of human acid-beta-glucosidase, the defective enzyme in Gaucher disease. *EMBO Rep* 4(7):704–709.
18. Cormand B, et al. (1998) Mutation analysis of Gaucher disease patients from Argentina: High prevalence of the RecNciI mutation. *Am J Med Genet* 80(4):343–351.
19. Kawame H, Eto Y (1991) A new glucocerebrosidase-gene missense mutation responsible for neuronopathic Gaucher disease in Japanese patients. *Am J Hum Genet* 49(6):1378–1380.
20. Zhao Y, Ren J, Padilla-Parra S, Fry EE, Stuart DI (2014) Lysosome sorting of β-glucocerebrosidase by LIMP-2 is targeted by the mannose 6-phosphate receptor. *Nat Commun* 5:4321.
21. Düsterhöft S, et al. (2015) Extracellular juxtamembrane segment of ADAM17 interacts with membranes and is essential for its shedding activity. *Biochemistry* 54(38):5791–5801.
22. Frankel AD, Pabo CO (1988) Cellular uptake of the tat protein from human immunodeficiency virus. *Cell* 55(6):1189–1193.
23. Horst M, Knecht EC, Schu PV (1999) Import into and degradation of cytosolic proteins by isolated yeast vacuoles. *Mol Biol Cell* 10(9):2879–2889.
24. Mazzulli JR, Zunke F, Isacson O, Studer L, Krainc D (2016) Alpha-synuclein-induced lysosomal dysfunction occurs through disruptions in protein trafficking in human midbrain synucleinopathy models. *Proc Natl Acad Sci USA* 113(7):1931–1936.
25. Liou B, et al. (2006) Analyses of variant acid beta-glucosidases: Effects of Gaucher disease mutations. *J Biol Chem* 281(7):4242–4253.
26. Grace ME, Graves PN, Smith FI, Grabowski GA (1990) Analyses of catalytic activity and inhibitor binding of human acid beta-glucosidase by site-directed mutagenesis. Identification of residues critical to catalysis and evidence for causality of two Ashkenazi Jewish Gaucher disease type 1 mutations. *J Biol Chem* 265(12):6827–6835.
27. Atrian S, et al. (2008) An evolutionary and structure-based docking model for glucocerebrosidase-saposin C and glucocerebrosidase-substrate interactions - relevance for Gaucher disease. *Proteins* 70(3):882–891.
28. Lieberman RL (2011) A guided tour of the structural biology of Gaucher disease: Acid-β-glucosidase and saposin C. *Enzyme Res* 2011:973231.
29. Sly WS, Kaplan A, Achord DT, Brot FE, Bell CE (1978) Receptor-mediated uptake of lysosomal enzymes. *Prog Clin Biol Res* 23:547–551.
30. Stahl PD, Rodman JS, Miller MJ, Schlesinger PH (1978) Evidence for receptor-mediated binding of glycoproteins, glycoconjugates, and lysosomal glycosidases by alveolar macrophages. *Proc Natl Acad Sci USA* 75(3):1399–1403.
31. Pastores GM, et al. (2004) Therapeutic goals in the treatment of Gaucher disease. *Semin Hematol* 41(4, Suppl 5):4–14.
32. Liou B, Haffey WD, Greis KD, Grabowski GA (2014) The LIMP-2/SCARB2 binding motif on acid β-glucosidase: Basic and applied implications for Gaucher disease and associated neurodegenerative diseases. *J Biol Chem* 289(43):30063–30074.
33. Benito JM, García Fernández JM, Ortiz Mellet C (2011) Pharmacological chaperone therapy for Gaucher disease: A patent review. *Expert Opin Ther Pat* 21(6):885–903.
34. Patnaik S, et al. (2012) Discovery, structure-activity relationship, and biological evaluation of noninhibitory small molecule chaperones of glucocerebrosidase. *J Med Chem* 55(12):5734–5748.
35. Pearson K (1909) Determination of the Coefficient of Correlation. *Science* 30(757):23–25.